S1 SE9800287

Studsvik Report

Current State of Knowledge in Radiolysis Effects on Spent Fuel Corrosion

Hilbert Christensen
Sham Sunder

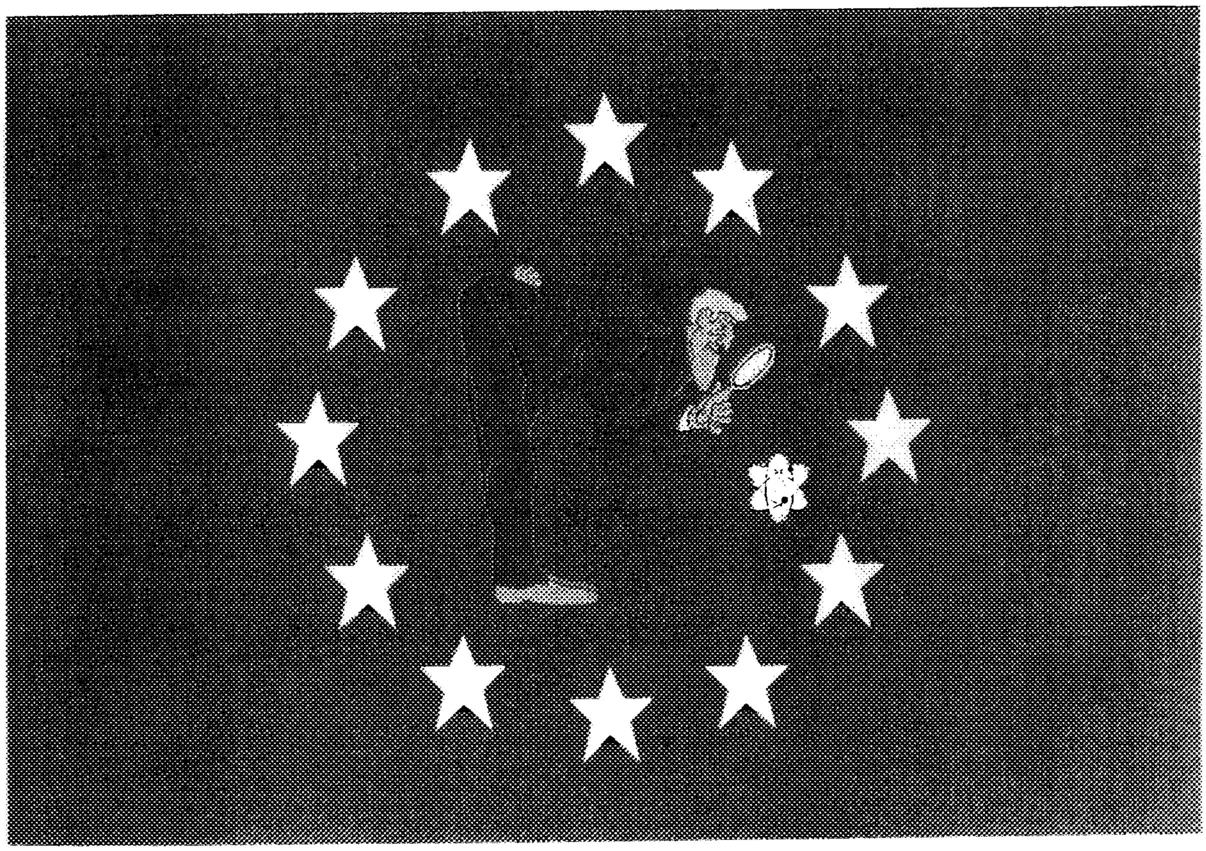

Studsvik Material

29 - 48

STUDSVIK MATERIAL AB

STUDSVIK/M-98/71

1998-09-27 6909

F14W-CT95-0004

Hilbert Christensen
Sham Sunder*

EU, AECL, SKB

Current State of Knowledge in Radiolysis Effects on Spent Fuel Corrosion

Abstract

Literature data on the effect of water radiolysis products on spent fuel oxidation and dissolution have been reviewed. Effects of γ-radiolysis, α-radiolysis, and dissolved O_2 or H_2O_2 in unirradiated solutions have been discussed separately. Also the effect of carbonate in γ-irradiated solutions and radiolysis effects on leaching of spent fuel have been reviewed. In addition a radiolysis model for calculation of corrosion rates of UO_2, presented previously, has been discussed. The model has been shown to give a good agreement between calculated and measured corrosion rates in the case of γ-radiolysis and in unirradiated solutions of dissolved oxygen or hydrogen peroxide. The model has failed to predict the results of α-radiolysis. In a recent study it was shown that the model gave a good agreement with measured corrosion rates of spent fuel exposed in deionized water.

Reviewed by

Approved by

---

* Atomic Energy of Canada Ltd

List of contents

1 Introduction

The concept of geological disposal of used nuclear fuel in corrosion resistant containers is being investigated in several countries, including Canada, Finland, Germany, Spain, Sweden, and U.S.A [1-15]. The purpose of the disposal concept is to minimize and delay the entry of radionuclides into the biosphere so that their effects on man and the environment are negligible. Transport by groundwater is the most likely pathway for radionuclides to migrate from the used fuel in the disposal vault to the biosphere.

The release rate of radionuclides in the fuel will depend upon the dissolution rate of the used fuel. Used nuclear fuel is mainly UO_2 ($\geq 95\%$), which has a very low solubility in water under reducing conditions [16,17]. Although groundwaters are generally reducing at the expected depth of a disposal vault [18], the redox conditions may be altered because of radiolysis of water by ionizing radiation associated with the fuel, as the radiolysis of water produces both oxidants and reductants [19-20]. The importance of radiolysis for oxidation and dissolution of UO_2 has been discussed previously [1, 3, 4, 10, 12].

We are developing a kinetic model, based on one proposed by Christensen and Bjergbakke (CB) [1], to predict the oxidation rates of UO_2 fuel due to water radiolysis [11,12]. This model assumes that molecules present in the surface of the fuel can react with the oxidants and reductants present in a water layer near the fuel surface. The thickness of this water layer is assumed to be equivalent to the diffusion path of the radicals formed during radiolysis.

In the present report a review is given of radiolysis effects, including discussions of the effects of γ- and α-radiation, of O_2 and H_2O_2 (without irradiation) and of carbonate. Effects of radiolysis have been noticed in some studies of spent fuel leaching.

2 Effect of γ-radiolysis

It was shown already in 1981 [21] that the dissolution rates of UO_2 and U_3O_8 were increased by γ-radiation, when samples were immersed in aqueous solutions of carbonate (pH 10) or H^+ (0.1 N H_2SO_4). At a dose rate of 1 $Gy{\cdot}s^{-1}$ the dissolution rate of UO_2 in carbonate (pH 10) increased by $2x10^{-7}$ $mg{\cdot}m^{-2}{\cdot}min^{-1}$ ($3.5x10^{-4}$ $\mu g{\cdot}cm^{-2}{\cdot}d^{-1}$). The dissolution rate increased with increasing dose rates. A systematic study of the effect of the various water radiolysis products on UO_2 oxidation and dissolution has been carried out by Sunder et al [3, 4, 9-11]. Different scavengers were used to optimize the production of specific radicals:

A solution saturated with N_2O favours the formation of OH radicals, as N_2O scavenges hydrated electrons to form OH radicals:

$$H_2O + e^-_{eq} + N_2O \rightarrow N_2 + OH^- + OH \quad (1)$$

A solution with mainly O^-_2 radicals was obtained by radiolysis of oxygenated solutions containing either t-butanol, $(CH_3)_3COH$, or formate ions, $HCOO^-$, as explained in reactions 2 through 5:

$$OH+(CH_3)_3COH \rightarrow H_2 + (CH_3)_2(CH_2)COH \quad (2)$$

$$OH + HCOO^- \rightarrow CO^-_2 + H_2O \quad (3)$$

$$CO^-_2 + O_2 \rightarrow CO_2 + O^-_2 \quad (4)$$

$$e^-_{aq} + O_2 \rightarrow O^-_2 \quad (5)$$

The formate and t-butanol are used to scavenge the OH radicals. Thus, in formate-containing solutions, O^-_2 radicals are formed by two reactions, i.e., the reactions of O_2 with e^-_{eq} and CO^-_2 radicals, respectively. In t-butanol solutions, the O^-_2 radicals are formed mainly by the reactions of O_2 with e^-_{eq}. Therefore, to a first approximation, the number of O^-_2 radicals formed in formate-containing solutions is twice the number of O^-_2 radicals formed in the solutions containing t-butanol under the same conditions [12]. However, the use of formate also results in the formation of CO_2, and hence CO^{2-}_3, an anion known to accelerate the oxidative dissolution of uranium oxides [21]. Note, O^-_2 is the basic form of HO_2 with a pK_a of 4.8. Experiments were also carried out in Ar-purged solutions, with no scavenger, resulting in the formation of a mixture of OH and e^-_{eq} radicals, and in O_2-saturated solutions, with no scavenger, to produce a mixture of OH and O^-_2 radicals.

* LET = Linear Energy Transfer

The specific effects of O_2 and H_2O_2 were studied by purging with oxygen, respectively by addition of H_2O_2 to unirradiated solutions, see Section 5.

The dose rate of the irradiated solutions were varied between 1 and 300 Gy/h using a ^{192}Ir gamma source ($t_{½}$= 74 days). The oxidation of UO_2 was monitored by recording the open-circuit corrosion potential (E_{CORR}) of the UO_2 electrode as a function of time.

The thickness of the film formed on the UO_2 electrode, as a result of oxidation during radiolysis, was determined by measuring the cathodic charge, Q_F, needed to reduce the film in cathodic-stripping voltammetry (CSV). An additional freshly polished UO_2 pellet was placed in the electrochemical cell to determine by XPS the surface composition of the oxidized layer formed on UO_2 during radiolysis.

Figures 1 and 2 show the corrosion potential of UO_2 measured as a function of time in Ar-purged or oxygenated 0.1 mol $\cdot l^{-1}$ $NaClO_4$ solution (pH=9.5) at various absorbed dose rates. The aerated solution also contained 0.01 mol l^{-1} sodium formate to maximize the concentration of O_2^- radicals, reactions [3] and [4]. In both solutions, E_{CORR} rose rapidly with time, this rise being faster in aerated than in Ar-purged solutions, see Figures 1B and 2B. Also, the effect of absorbed dose rate is apparent for lower potentials in aerated than in Ar-purged solutions. At the lowest dose rates used for each solution, the rise of E_{CORR} was arrested over the potential range $-500mV < E_{CORR} \leq -100mV$ SCE in both Ar-purged and oxygenated solutions.

The shape of the curves in Figures 1 and 2 suggests that oxidation of the UO_2 electrode surface occurs in two separate stages: (a) stage 1 up to ~ - 100 mV SCE, in which E_{CORR} rises approximately exponentially with time; and (b) stage 2, above ~ -100 mV SCE, in which E_{CORR} changes are approximately linear with time until the final approach to steady state. These stages are more distinct in oxygenated solutions, Figure 2, as is the dose-rate dependence of stage 2.

The attainment of steady state can take from ~2 to ~28 h, depending on the solution redox potential (i.e., whether oxygen is present) and the absorbed dose rate. The importance of even small concentrations of radiolysis products is exemplified by the difference between steady-state E_{CORR} values recorded at low dose rates and those recorded in either unirradiated Ar-purged solution, Figure 1A, or unirradiated aerated solution, Figure 2A. Once a steady-state E_{CORR} is achieved, switching off the radiation field produces only a minor decrease in E_{CORR}, Figure 1A, confirming that stage 2 of oxidation is irreversible.

* LET = Linear Energy Transfer

Steady-state values of E_{CORR} are plotted as a function of the logarithm of absorbed dose dose rates in Figure 3. This plot includes values measured in N_2O-purged solutions, as well as in aerated solutions containing t-butanol. The shaded areas show the range of steady-state E_{CORR} values recorded on other UO_2 electrodes in many previous experiments in aerated or Ar-purged solution [22-25]. The steady-state E_{CORR} values achieved in the presence of gamma radiation are higher than those achieved in either aerated solutions [22] or solutions containing hydrogen peroxide [24,25], strongly suggesting that oxidation and dissolution of the UO_2 by radiolytically produced radicals is significant.

The increase in corrosion rates caused by the radiation field is also demonstrated in Figures 4 and 5. Calculations have shown that the concentration of H_2O_2 is decreased, when the gamma field is introduced. At the same time (see Figure 5) the corrosion rate is increased, clearly demonstrating that the radicals produced by radiolysis are more effective than H_2O_2 in oxidation of UO_2.

Figure 6 shows the cathodic charge (Q_F) measured by CSV as a function of the value of E_{CORR} achieved by the time the experiment was terminated. The plot includes E_{CORR} values measured in all four of the solutions over a wide range of absorbed dose rates and for various durations of experiment. In many cases, the E_{CORR} values are not steady-state values. Q_F is a measure of the thickness of the oxidized films formed on the electrode surface. The thickness of these films is directly related to E_{CORR}, up to ~0 mV, irrespective of the composition of the solution (i.e., the nature of the predominant radiolytic oxidant) or whether the oxidation was achieved rapidly or slowly. At higher potentials, even though a steady-state E_{CORR} is achieved, the thickness of the oxidized surface film continues to increase.

Figure 7 shows the U^{VI}:U^{IV} ratio obtained by XPS analysis of UO_2 specimens exposed to the same solutions for equivalent times [26,27]. Consequently, the surface composition of these specimens is expected to reflect that of the electrodes. This ratio increases slowly over the E_{CORR} range -400mV to -100mV SCE, during which the film thickness increases linearly with time, Figure 6. Once steady-state E_{CORR} values are achieved around -100 mV SCE, the film thickening that occurs at these potentials, Figure 6, is accompanied by a large increase in U^{VI}:U^{IV}, demonstrating that U^{VI} oxides form at these potentials.

* LET = Linear Energy Transfer

The oxidation of UO_2 in the presence of oxidants produced by the gamma radiolysis of water occurs in two distinct stages:

(1) The formation of a thin layer of UO_{2+x} with a stoichiometry close to $UO_{2.33}$. This process occurs over the potential range -500 mV<E_{CORR} ≤-100 mV SCE.

(2) The subsequent oxidative dissolution of this surface layer to produce soluble U^{VI} species and secondary phases, probably hydrated schoepite ($UO_3 \cdot xH_2O$), on the electrode surface. This process starts around E_{CORR} ~-100 mV SCE and eventually achieves steady state at a value of E_{CORR} determined by the absorbed dose rate.

In unirradiated aerated solutions, the formation of secondary phases appears to be concentrated initially in grain boundaries [22]. Their confinement to these sites made them slow to redissolve when the solutions were subsequently purged with nitrogen. A similar concentration of hydrated UO_3 phases at grain boundaries, and their subsequent slow redissolution could explain the slow relaxation in E_{CORR} observed in formate solutions once the radiation field is switched off.

Using an electrochemistry-based dissolution model [6] an experimental dissolution rate was deduced from the measured steady-state corrosion potential.

The following equation may be used:

$$CR = 78 \cdot E(-4.4 + 16 \times E_{CORR})$$

where

CR is the corrosion rate in $\mu g \cdot cm^{-2} \cdot d^{-1}$,

E means exponent of 10, and

E_{CORR} is the corrosion potential in V SCE.

Corrosion rates were measured and compared with calculated values using a model described below, Section 4, see Table 1. The experimental results varied between 10^{-4} $\mu g \cdot cm^{-2} \cdot d^{-1}$ in Ar-purged solutions irradiated at 5 $Gy \cdot h^{-1}$ up to 0.75 $\mu g \cdot cm^{-2} \cdot d^{-1}$ in O_2-purged solutions irradiated at 280 $Gy \cdot h^{-1}$.

In experiments by Christensen the oxidation and dissolution of UO_2 pellets immersed in γ-irradiated water was measured [28], using various scav-

* LET = Linear Energy Transfer

engers. The composition and thickness of the oxidized surface layer were measured using SIMS and XPS. Uranium in solution and on walls were measured by chemical analysis. The corrosion rate caused by OH and O_2^- radicals was about 3 $\mu g \cdot cm^{-2} \cdot d^{-1}$ at a dose rate of 600 $Gy \cdot h^{-1}$, see Table 1.

3 Effect of α-radiolysis

The effect of products from α-radiolysis of water on UO_2 oxidation and dissolution has been studied by Shoesmith, Sunder et al [6, 24, 29-31]. Since α-activity within used fuel decays slowly in comparison with γ- and β-activity, there is a possibility that oxidative dissolution will be sustained by α-radiolysis for a long time.

Corrosion potentials were measured in a thin-layer elctrochemical cell that allows an α source of known strength to be brought within ~25 μm of a UO_2 electrode [24]. Using steady-state E_{CORR} values measured for α sources of various strengths, values for the dissolution rate as a function of α source strength have been obtained in Ar-purged solution.

The results for various α-sources are given in Table 2. The corrosion rates are considerable lower than for comparable γ dose rates, see Table 1. The difference may partly be explained by the difference in initial radiolysis yields, as seen from Table 4. For low-LET* radiation such as γ and β the yields of radicals are high and the yields of molecules (H_2 and H_2O_2) are low. The opposite is true for high-LET radiation such as α. Therefore, the effect of α-radiolysis may be caused mainly by H_2O_2, the oxidizing effect of which has been found to be considerably lower than the effect of the radicals OH and O_2^-. In the experiments an α-source was placed about 30 μm from the UO_2 electrode. When the separation distance was increased to 750 μm, the corrosion rate decreased by almost two orders of magnitude. The interpretation given was that H_2O_2 caused corrosion in the narrow gap but it was swept out by diffusion when the gap was opened. At the larger distance radiolysis products did not reach the electrode. Thus, it seems likely that the behaviour of UO_2 in the presence of α-radiolysis will be similar to its behaviour in H_2O_2.

Sunder et al [27] studied the effect of alpha radiolysis of water on the oxidation and dissolution of UO_2 at 100 °C as a function of α-field strength and water chemistry using X-ray photoelectron spectroscopy. In N_2-purged solutions the oxidation of UO_2 increased with the strength of the α-flux: an α-flux greater than or equal to that from a 250-μCi americium-241 source led to oxidation of UO_2 beyond the $UO_{2.33}$ (U_3O_7) stage, and an α-flux equal to that from a 5-μCi source did not result in UO_2 oxidation beyond the $UO_{2.33}$ stage. The presence of dissolved H_2 in water at a concentration $\geq 1.6 \times 10^{-4}$ mol dm^{-3} reduced the oxidation and dissolution of UO_2 due to α-radiolysis at temperature ≥100°C. In the solutions containing H_2 the oxidation did not increase with increasing dose rate.

* LET = Linear Energy Transfer

It was concluded that α-radiolysis caused by 500 y old CANDU fuel (corresponding to an α-flux of $5\mu Ci \cdot cm^{-2}$) would not cause oxidation beyond the $UO_{2.33}$ stage and hence not cause increased dissolution.

4 Modelling

γ- and β-radiolysis

Christensen and Bjergbakke [1] have presented a mechanistic model for UO_2 oxidation caused by water radiolysis products. The model is based on three assumptions:

- Only the species which are produced in the water within one diffusion length from the UO_2 surface can react with UO_2.
- The heterogeneous reaction could be substituted with a homogeneous one, assuming that the UO_2 reacts as if one monomolecular layer of UO_2 is dissolved within the range of the radicals.
- The rate of the heterogeneous reactions of U-species are similar to known rates of homogeneous reactions of metal ions in water.

Based on these assumptions a model was set up, including reactions of water radiolysis products between themselves. The model was tested against experiments by Gromov [21] and a fair agreement was obtained between measured and calculated corrosion rates.

The kinetic model was further developed and optimized for the neutral solution conditions expected in groundwaters. This refinement was based on a series of electrochemical open-circuit corrosion experiments [3, 4, 10], mainly using a gamma source, see Section 2.

A schematic diagram illustrating the general change in the corrosion potential with time for neutral solutions, and indicating the progression in the oxidation and dissolution process with corrosion potential, is shown in Figure 8.

The process can be divided into two distinct stages: (i) a transitory stage during which the surface is oxidized to approximately $UO_{2.33}$, (ii) a steady-state stage during which dissolution (as U^{VI}) occurs at a constant rate from a surface layer of $UO_{2.33}$ (5-8 nm thick). At sufficiently large oxidant concentrations, reprecipitation of U^{VI} to yield secondary phase ($UO_3 \cdot 2H_2O$) can occur [23].

We have commonly taken the time for the potential to reach a value of -100 mV SCE as an approximate measure of the rate of formation of this $UO_{2.33}$ layer [32]. The appropriate corrosion (dissolution) rate is that obtained once steady-state dissolution conditions have been established, *i.e.*

once the corrosion potential $(E_{CORR})_{SS}$ has been attained (Figure 8). At this potential the current for the oxidative dissolution of UO_2 is counterbalanced by an equal and oppo-site current for the oxidant reduction. It is this value for the E_{CORR} which is used in our electrochemical model to obtain a value for the corrosion rate. For disso-lution in aerated solutions the rate-controlling step appears to be the reduc-tion of oxygen, a notoriously slow reaction [33]. For radiolytic oxidants (O_2^-, OH, H_2O_2), electron transfer to the oxidant will be much faster, and the rate of the overall process is more likely to be controlled by the anodic dis-solution step.

As mentioned above the thickness of the water layer is assumed to be equal to the diffusion range χ of the reacting radicals. This range is estimated from the calculated lifetime of radiolytically generated species at a specific dose rate [34]. For the OH radicals, χ varies from 16 µm at a dose rate of 280 Gy h^{-1} to 44 µm at 5 Gy h^{-1}. Since this dependence of diffusion range on dose rate is only to the power –0.25 for the dose-rate range in our experi-ments, we have taken it to be constant at 25 µm. Thus, the initial concentra-tion of UO_2 is set at a value of $5 \cdot 10^{-4}$ mol l^{-1}, which corresponds to the dis-solution of a monolayer of UO_2 in a water layer of approximately 25 µm thickness [1].

The reaction mechanism and rate constants used in our refined model are given in Table 3 and G-values are given in Table 4. Some of the changes from the original model are discussed below:

- The reversible formation of U^V species (denoted UO_3H in Table 3) can be assumed to represent the reversible formation of the intermediate $UO_{2.33}$ film. This film reaches a steady-state thickness equivalent to a steady-state concentration of U^V in our model.

- The formation of the $UO_{2.33}$ surface film leads to a decrease in the oxidation rate as it thickens. This is brought about in the model by decreasing the concentration of UO_2 with time (reactions 59 and 60 in Table 3).

- The rate constants for oxidation by H_2O_2 (reactions 36 and 42) were lowered relative to those for radicals in agreement with experimental observation.

- Reactions with arbitrary rate constants were added to represent decomposition of H_2O_2 on the UO_2 surface (*i.e.* reaction 54).

- Reactions to represent the slow oxidation of UO_2 by dissolved O_2 in the absence of a radiation field were added (reactions 57 and 58).

- The experimental rates with which the predictions of this model are to be compared were determined in an open system making it necessary to include rate constants for the removal of gases (O_2, H_2) from the system (reactions 52 and 53).

Model calculations were carried out using the computer program MAKSIMA-CHEMIST [35], and these calculations are compared with results from electrochemical experiments in Tables 1 and 5.

Table 5 compares the times taken to reach 90% of the steady-state concentration of UO_3H species with the experimental times to reach an open-circuit corrosion potential of −100 mV SCE. Table 1 compares the calculated and measured corrosion (dissolution) rates for UO_2. Experimental corrosion rates were obtained from values of $(E_{CORR})_{SS}$ using our electrochemistry-based model [6, 36]. Calculated dissolution rates were obtained from concentration-time profiles predicted by the model. Figure 9 shows two such sets of calculated profiles for Ar-purged solutions, at initial pH 9.5, undergoing gamma radiolysis at dose rates of 5 and 280 Gy h^{-1} respectively. Dissolution rates were obtained from the linear increase in dissolved U^{VI} (UO_3D) over the period 20-30 h, as indicated in Figure 9.

For high dose rates the model predicts quite accurately the rate of oxidation of the UO_2 surface to $UO_{2.33}$, i.e. the predicted time to reach 90% of the steady-state concentration of U^V (UO_3H) is in good agreement with the measured time to reach −100 mV SCE, Table 5.

The largest discrepancy between measured and predicted rates in irradiated solutions is for measurements in N_2O-purged solutions. In this case, the experimental values are suspect owing to unusual potential-time curves [10].

The agreement between calculated and electrochemically measured corrosion (dissolution) rates is generally good, see Table 1. It should be noted that significant uncertainty is associated with the extrapolation required to calculate dissolution rates from electrochemical data.

α-radiolysis

It was not possible to predict the corrosion rate of UO_2 in solutions undergoing α-radiolysis using the mechanistic model discussed above. The predicted corrosion rates were orders of magnitude higher than the electrochemically measured values, see Table 2. In addition the dose rate (DR) dependence is lower for the calculated values ($\approx DR^{1.0}$) than for the measured values ($\approx DR^{1.8}$).

Obviously, the model is lacking one or more parameters which are of decisive importance in the experiments.

Spent fuel

The dissolution rates of spent fuel have been predicted using an *empirical* model [6, 36, 37]. This model is based on corrosion rates measured electrochemically both using gamma and alpha irradiation.

Predictions have been made both for CANDU fuel and for LWR fuel, see Figures 10-13. From these figures it can be deduced that oxidative dissolution of CANDU fuel (Burnup 685 GJ $\cdot$ kg^{-1} U) should not take place for fuel older than 500 y. The corresponding time limit for LWR fuel (Burnup 45 Mwd $\cdot$ kg^{-1} U) is about 30 000 y.

An attempt has been made to use the *mechanistic* model to predict the corrosion rate of spent fuel [38]. The predicted corrosion rates for LWR fuel (45 MWd $\cdot$ kg^{-1}) varied between $2 \cdot 10^{-3}$ and 0.5 μg $\cdot$ cm^{-2} $\cdot$ d^{-1}. At storage times of 10^4, 10^5 and 10^6 y, the predicted dissolution rates were 0.1, 0.01 and $5 \cdot 10^{-3}$ μg $\cdot$ cm^{-2} $\cdot$ d^{-1} respectively considerably higher than values predicted by the empirical model, see Figure 13.

5 Effect of O_2 and H_2O_2 in unirradiated solutions

Although the effect of O_2 and H_2O_2 in unirradiated solutions is not directly related to radiolysis, the systems can give information useful for evaluation of the effect of radiolysis. The effect of α-radiolysis is sometimes assumed to be the same as the effect of H_2O_2.

Effects of dissolved O_2

Several workers have studied the effects of dissolved oxygen on UO_2 dissolution rates. Recent reviews of these studies are given in Refs 36, 39-41. Figure 14 shows the corrosion rates of UO_2 in non-complexing solutions at pH ~9 as a function of the dissolved oxygen concentration, as reported by Shoesmith and Sunder [36]. This figure also includes recent results of Casas et al [42] and Grambow et al [41] for comparison purposes. Although the results of Shoesmith and Sunder were obtained using their electrochemical model, and those of Casas et al and Grambow et al were obtained by directly measuring the amounts of dissolved uranium in the solution, there is a good agreement between these results. It should be mentioned here that Grambow et al have misrepresented the results of Shoesmith and Sunder in comparing their results with those of Shoesmith and Sunder. Grambow et al have plotted the data of Shoesmith and Sunder (Figure III.8 in their report [41]) using same numerical values (Figure 9 in Ref 36) although Shoesmith and Sunder used units of $\mu g \cdot cm^{-2} \cdot d^{-1}$ while Grambow et al use units of $mg \cdot m^{-2} \cdot d^{-1}$!

The results shown in Figure 14 suggest a first-order relationship between the dissolution rates and dissolved-oxygen concentration. This conclusion is in agreement with the results of Grandstaff [43] and of Thomas and Till [44]. However, there are several other studies that have reported values of less than 1 for the reaction order with respect to oxygen concentration [41]. A reaction order of ~0.5 was reported by Hocking et al [45] during their investigations of O_2 reduction on an electrode made of unusual UO_2 pellet; and several used-fuel dissolution studies have reported a reaction order of less than 1.0 (see Ref 46 and references therein). It should be noted here that it is difficult to determine reaction order with respect to oxygen, from the studies with irradiated UO_2 (used fuel) samples as one cannot separate the effects from the dissolved oxygen from those of the water-radiolysis products formed by the ionizing radiation associated with the used fuel. It has been shown above that the radiolysis of water increases the rate of UO_2 dissolution.

Effects of H_2O_2

Shoesmith and Sunder have studied effects of H_2O_2, as a function of concentration, on UO_2 dissolution [36]. Figure 15 shows their rates of dissolution of UO_2 as a function of H_2O_2 concentration in non-complexing solutions, pH ~9. This figure also shows the results of Christensen et al [47], Gimenez et al [48] and Grambow et al [41] for comparison purposes. The results of Shoesmith and Sunder [36] are from electrochemical measurements while those of other workers were obtained by chemically measuring the amounts of dissolved uranium in the solution. There is a fair agreement between the results of Shoesmith and Sunder with those of Christensen et al [47] and Gimenez et al [48]. The agreement between the results of Grambow et al with other results is not as good, given in the report by Grambow et al [41]. Grambow et al have made the same error in using the results of Shoesmith and Sunder for the effects of H_2O_2 as the one they made in using their O_2 results, i e they have used the data from Ref 36 in their figures (Figures III.5 and III.8 in their report [41]) without converting the units (see above).

A comparison of the results shown in Figures 14 and 15 suggests that the dissolution rates are similar in solutions containing oxygen or H_2O_2 at comparable concentrations. This is despite the fact that the oxidation reaction

$UO_2 \rightarrow UO_{2.33}$

is supposed to be much faster (by a factor of around 200) in H_2O_2 than that in the oxygenated solutions [24, 25, 37]. The similarity of the dissolution rates in H_2O_2 and oxygenated solutions, at comparable concentrations, suggestes that the dissolution reaction

$UO_{2.33} \rightarrow UO_2^{2+}$

is slow in both solutions.

Figure 15 suggests three distinct regions of behaviour of UO_2 dissolution rates as a function of H_2O_2 concentration [36], i e,

(a) for $[H_2O_2] > 5 \times 10^{-3}$ mol·dm^{-3}, the dissolution rate increases with the peroxide concentration with approximately first-order dependence;

(b) for $2 \times 10^{-4} < [H_2O_2] < 5 \times 10^{-3}$ mol· dm^{-3}, the dissolution rate is independent of the peroxide concentration; and

(c) for $[H_2O_2] < 2 \times 10^{-4}$ mol dm^{-3}, the dissolution rate falls rapidly.

It has been proposed that the hydrogen peroxide decomposition to oxygen and water in the intermediate concentration range competes with the oxidative dissolution reaction [24, 25]. Therefore, it is essential to include a peroxide decomposition step to model the effects of H_2O_2 on dissolution rates. Details of our attempts to include the hydrogen peroxide decomposition reactions in our model to calculate radiolysis effects are given in Ref 49.

Sunder et al have studied the effects of pH on UO_2 the oxidation by H_2O_2 [25]. They observed an increase in UO_2 oxidation rate with a decrease in solution pH.

6 Effect of carbonate in irradiated solutions

The presence of complexing anions increase the oxidative dissolution rates of UO_2 by increasing the rate of removal of uranyl species (UO_2^{2+}) from the surface to the solution. As carbonate ions form strong complexes with uranyl ions, the effects of carbonate on UO_2 oxidation have been studied by several workers. Some recent reviews of these investigations are given in Ref 39, 40 and 46. It has been shown that the UO_2 dissolution reaction order with respect to carbonate is dependent on the carbonate concentrations. Its value is generally much less than 1, and values as low as 0.25 have been reported [46]. Further studies are required to model the effects of the presence of carbonate on UO_2 fuel oxidation in carbonate containing solutions undergoing radiolysis. Radiolysis produces carbonate radicals (CO_3) which can react like OH radicals in oxidation reactions. Our initial attempts to model the effect of carbonate containing solutions undergoing radiolysis on fuel oxidation are summarized in Ref 50.

7 Radiolysis effects on leaching of spent fuel

Loida et al [51] measured gas generation rates from radiolysis during spent fuel dissolution. In most cases hydrogen and oxygen were produced in a near stoichiometric ratio. The gas production was not increased significantly when fuel powder (grain size 3 μm) was used. The interpretation of this was that radiolysis gases were produced by γ- and not by α-radiation. In the presence of iron powder the hydrogen production was increased by about one order of magnitude and the measured oxygen production was close to zero. The fuel alteration rate was increased when powder was used and decreased in the presence of iron powder. In 95 % saturated NaCl solution the hydrogen production (HP) was higher and the fuel alteration (FA) lower than in deionized water: HP/FA was 15 and 3, respectively. When powder was used (in NaCl solution) the ratio HP/FA was about 2.4. Thus the fuel alteration rate was only 2.4 - 15 times lower than the production rate of hydrogen from radiolysis. Obviously oxidants, produced by radiolysis, play a significant role in oxidation of the fuel. From the experiments it is not possible to deduce a total stoichiometric balance of products.

Dose rate in water from α- and γ-radiation was not given in the report but some details have been given previously [52]. LWR fuel with a burnup >50 MWd/kg U was used. Inside a thin crack in 1 - 10 y old fuel α-dose rates of about 3000 Gy/h and β-dose rates of 9000-80000 Gy/h may be expected [53]. The α-dose rates on an open surface may be expected to be about half of the α-dose values inside the thin crack (irradiation from only one side).

It is essential to know the dose rates in water layers in contact with UO_2 in order to predict dissolution rates of used fuel in a disposal vault caused by water radiolysis [54]. Sunder has calculated the alpha, beta and gamma dose rates, in contact with a reference used CANDU fuel, as a function of time, and described a procedure to calculate the dose rates in fuels of other burnups [55]. The dose rate information combined with the knowledge of fuel dissolution rates, as a function of dose rate, enables one to predict the dissolution rates of used fuel as a function of its cooling time. Johnson et al have used this information to calculate the dissolution rates of used CANDU fuel, in contact with groundwater, in a defective copper container [56]. They concluded that beta radiolysis of water is the main cause of oxidation of used CANDU fuel in a failed container and that the use of a corrosion model is required for ~1000 a of emplacement in the waste vault.

With the model presented above it is possible to calculate the fuel dissolution rates as a function of dose rate and groundwater chemistry. Combining this knowledge with the dose rate information, one should be able to predict the dissolution rate of any used fuel.

Thus, the model was used to calculate the oxidation of UO_2 and the gas production, simulating the experiments of Loida et al [51], describe above.

The system was divided into four phases, see Figure 16, requiring three separate calculations.

Phase 1: a 30-µm-thick surface layer on top of the pellet, irradiated by α-, β- and γ-radiation.

Phase 2: a 0.3-cm layer on top of phase 1, irradiated by β- and γ-radiation.

Phase 3: the rest of the solution, irradiated by γ-radiation.

Phase 4: the gas phase, unirradiated.

The conclusion of the calculations [57] were that the UO_2 corrosion was caused only by radiolysis in the thin surface layer on top of the surface (phase 1) and the gas production was caused almost exclusively by γ-radiolysis in the bulk water (phase 3). The calculated fuel alteration rate was 2.2×10^{-8} mol $UO_2 \cdot (gU)^{-1} \cdot day^{-1}$, about three times higher than the experimental rate, 6.3×10^{-9} mol $UO_2 \cdot (gU)^{-1} \cdot day^{-1}$.

Acknowledgement

This work was done under the EU contract F14W-CT95-0004 and the Canadian Nuclear Fuel Waste Management Program, which is funded by AECL Research and Ontario Hydro under the auspices of the CANDU Owners Group, COG-93-478. H Christensen acknowledges support from the Swedish Nuclear Fuel Management Co of Sweden.

References

1 CHRISTENSEN, H and BJERGBAKKE, E
Scientific basis for nuclear waste management X, editors J K Bates and W B Seefeldt, 1987.
Mat Res Soc Symp Proc 84, p 115.

2 JOHNSON, L H and SHOESMITH, D W
Radioactive waste forms for the future, editors W Lutze and R C Ewing, Elsevier Sci Publ B V., Amsterdam, 1988, p 635.

3 SUNDER, S, SHOESMITH, D W, CHRISTENSEN, H, BAILEY, M G AND MILLER, N H
Scientific basis for nuclear waste management XII, editors W Lutze and R C Ewing, 1989.
Mat Res Soc Symp Proc 127, p 317-324.

4 SUNDER, S, SHOESMITH, D W, CHRISTENSEN, H, MILLER, N H AND BAILEY, M G
Scientific basis for nuclear waste management XIII, editors V M Oversby and P W Brown, 1990.
Mat Res Soc Symp Proc 176, p 457.

5 FORSYTH, R S and WERME, L O
J Nucl Mater, 190 (1992):3.

6 SHOESMITH, D W and SUNDER, S
J Nucl Mater, 190 (1992):20.

7 GRAY, W J, LEIDER, H R and STEWARD, S A
J Nucl Mater, 190 (1992):46.

8 BRUNO, J, CASAS, I and SANDINO, A
J Nucl Mater, 190 (1992):61.

9 OLLILA, K
J Nucl Mater, 190 (1992):70.

10 SUNDER, S, SHOESMITH, D W, CHRISTENSEN, H and MILLER, N H
J Nucl Mater, 190 (1992):78.

11 CHRISTENSEN, H, SUNDER, S and SHOESMITH, D W
Calculations of radiolysis in connection with UO_2 oxidation studies. III. Adjustment of the final stage of oxidation.
Studsvik AB, Sweden 1990 (Technical Note NS-90/99).

12 CHRISTENSEN, H, SUNDER, S and SHOESMITH, D W
J Alloys Compounds, 213 (1994):93.

13 JOHNSON, L H, LENEVEU, D M, SHOESMITH, D W, OSCARSON, D W, GRAY, M N, LEMIRE, R J and GARISTO, N C
The disposal of Canada's nuclear fuel waste: The vault model for postclosure assessment.
Atomic Energy of Canada Limited 1994 (Report AECL-10714).

14 JOHNSON, L H, TAIT, J C, SHOESMITH, D W, CROSTHWAITE, J J and GRAY M N
The disposal of Canada's nuclear waste: Engineered barriers alternatives.
Atomic Energy of Canada Limited 1994 (Report AECL-10718.

15 GRAMBOW, B, LOIDA, A, DRESSLER, P, GECKEIS, H, DIAZ, P, GAGO, J, CASSAS, I, de PABLO, J, GIMENEZ, J and TORRERO, M E
Long-term safety of radioactive waste disposal: reaction of high burnup spent fuel and UO_2 in saline brines at room temperature.
Kernforschungszentrum, Karlsruhe, 1994 (KfK 5377).

16 PARKS, G A and POHL, D C
Geochim Cosmochim Acta, 52 (1988), p 863.

17 LEMIRE, R J and GARISTO, F
The solubility of U, Nb, Pu, Th and Tc in a geological disposal vault for used nuclear fuel.
Atomic Energy of Canada Limited 1989 (Report AECL-10009).

18 GASCOYNE, M and KAMINENI, D C
Groundwater chemistry and fracture mineralogy in the Whiteshell research area.. Supporting data for the geosphere and biosphere transport models.
Technical Record, Whiteshell Laboratories, Atomic Energy of Canada Limited 1992 (Report TR-516).

19 ALLEN, A O
The radiation chemistry of water and aqueous solutions.
D Van Nostrand Co. Inc., Princeton 1961.

20 SPINKS, J W T and WOODS, R J
An introduction to radiation chemistry, 3rd ed.
Wiley-Interscience, New York 1990.

21 GROMOV, V
Radiat Phys Chem, 18 (1981), p 135.

22 SHOESMITH, D W, SUNDER, S, BAILEY, M G and WALLACE, G J
Corrosion Science, 29 (1989), p 1115.

23 SUNDER, S, SHOESMITH, D W, LEMIRE, R J, BAILEY, M G and WALLACE, G J
Corrosion Science, 32 (1991):4, p 373.

24 SHOESMITH, D W, SUNDER, S, JOHNSON, L H and BAILEY, M G
Scientific basis for nuclear waste management IX, editor L O Werme, 1985.
Mat Res Soc Symp Proc 50, p 309.

25 SUNDER, S, SHOESMITH, D W, JOHNSON, L H, BAILEY, M G, WALLACE, G J and SNAGLEWSKI, A P
Scientific basis for nuclear waste management X, editors J K Bates and W B Seefeldt, 1987.
Mat Res Soc Symp Proc 84, p 102.

26 McINTYRE, N S, SUNDER, S, SHOESMITH, D W and STANCHELL, F W
J Vacuum Sci Technol, 18 (1981), p 714.

27 SUNDER, S, BOYER, G D and MILLER, N H
J Nucl Mater, 175 (1990), p 163.

28 CHRISTENSEN, H
Scientific basis for nuclear waste management X, editors J K Bates and W B Seefeldt, 1987
Mat Res Soc Symp Proc 84, p 213.

29 BAILEY, M G, JOHNSON, L H and SHOESMITH, D W
Corrosion Science, 25 (1985), p 233-238.

30 SUNDER, S, SHOESMITH, D W, JOHNSON, L H, WALLACE, G J, BAILEY, M G and SNAGLEWSKI, A P
Mat Res Soc Symp Proc 84, p 103, 1987.

31 SHOESMITH, D W, SUNDER, S, IKEDA, B M and KING, F
Mat Res Soc Symp Proc 127, p 279, 1989.

32 SUNDER, S, SHOESMITH, D W, MILLER, N H AND WALLACE, G J
Mat Res Soc Symp Proc 257, p 345, 1992.

33 HOCKING, W H, BETTERIDGE, J S and SHOESMITH, D W
The cathodic reduction of dioxygen on uranium oxide in dilute alkaline aqueous solution.
Atomic Energy of Canada Limited, Pinawa, Canada 1991 (Report AECL-10402).

34 CHRISTENSEN, H and SUNDER S
Calculations of radiolysis in connection with UO_2 oxidation studies. Studsvik Nuclear, Sweden 1989 (Technical Note NS-89/117).

35 CARVER, M B, HANLEY, D V and CHAPLIN, K R
MAKSIMA-CHEMIST, a program for mass action kinetics simulation by automatic chemical equation manipulation and integration using stiff techniques.
Atomic Energy of Canada Limited, Pinawa, Canada 1979 (Report AECL-6413).

36 SHOESMITH, D W and SUNDER, S
An electrochemistry-based model for the dissolution of UO_2.
SKB, Stockholm 1991 (SKB Tech. Rep., 91-63); also published by Atomic Energy of Canada Ltd., Pinawa, Canada 1991 (AECL-10488).

37 SUNDER, S, SHOESMITH, D W and MILLER, N H
Prediction of the oxidative dissolution rates of used nuclear fuel in a geological disposal vatul due to the alpha radiolysis of water. Scientific basis for nuclear waste management, editors T Murakami and R C Ewing, 1995.
Mat Res Soc Symp Proc 353, 1995, p 617-624.

38 CHRISTENSEN, H
Calculation of radiation induced dissolution of UO_2.
Studsvik Material AB, Sweden 1991 (Technical Report M-91/10).

39 SUNDER, S, and SHOESMITH, D W
Chemistry of UO_2 fuel dissolution in relation to the disposal of used nuclear fuel.
Atomic Energy of Canada Limited Report 1991, AECL-10395.

40 SHOESMITH, D W, SUNDER, S, and HOCKING, W H
Electrochemistry of UO_2 nuclear fuel.
Chapter XX. In Electrochemistry of Novel Materials, J Lipkowski and P N Ross (Eds), VCH Publishers (1994), 297-337.

41 GRAMBOW, B, LOIDA, A, DRESSLER, P, GECKEIS, H, DIAZ, P, GAGO, J, CASAS, I, de PABLO, J, GIMENEZ, J, and TORRERO, M E
Long-term safety of radioactive waste disposal: reaction of high burnup spent fuel and UO_2 in saline brines at room temperature.
Kernforschungszentrum Karlsruhe Report 1994 (KfK 5377).

42 CASAS, I, GIMENEZ, J, de PABLO, J, and TORRERO, M E
The dissolution of UO_2 in different redox conditions.
In Materials Research Society Symposia Proceedings 294 (Ed C G Interrante and R T Pabalan) (Scientific Basis for Nuclear Waste Management XVI) (1993) 617, 67-72.

43 GRANDSTAFF, D E
A kinetic study of the dissolution of uraninite.
Economic Geology 71 (8) (1976), 1493-1506.

44 THOMAS, G F, and TILL, G
The dissolution of unirradiated UO_2 fuel pellets under simulated disposal conditions.
Nuclear and Chemical Waste Management 5 (1984), 141-147.

45 HOCKING, W H, BETTERIDGE, J S and SHOESMITH, D W
Atomic Energy of Canada Limited Report 1991 (AECL-10402).

46 SHOESMITH, D W, TAIT, J C, SUNDER, S, GRAY, W J, STEWARD, S A, RUSSO, R E, and RUDNICKI, J D
Factors affecting the differences in reactivity and dissolution rates between UO_2 and spent nuclear fuels.
Atomic Energy of Canada Limited Report 1996 (AECL-11515, COG-95-581).

47 CHRISTENSEN, H, FORSYTH, R, LUNDQVIST, R, and WERME, L O
Radiation induced dissolution of UO_2.
Studsvik Energiteknik AB, Nyköping, Sweden 1990 (Studsvik Report NS-90/85).

48 GIMENEZ, J, BARAJ, E, TORRERO, M E, CASAS, I, and de PABLO, J
Nucl Mater 238 (1996), 64-80.

49 CHRISTENSEN, H and SUNDER, S
Calculation of radiation induced corrosion of UO_2. Adjustment of rate constants for reaction of O_2 and H_2O_2.
Studsvik Material AB, Nyköping, Sweden 1994 (Studsvik Report M-94/120).

50 CHRISTENSEN, H and SUNDER, S
Calculation of radiation induced corrosion of UO_2 in solutions containing carbonate.
Studsvik Material AB, Nyköping, Sweden 1996 (Studsvik Report M-96/4).

51 LOIDA, A, GRAMBOW, H, BECKEIS, H and DRESSLER, P
Processes controlling radionuclide release from spent fuel.
Scientific basis for nuclear waste management XVIII, editors T Murakami and R E Ewing, 1995.
Mat Res Soc Symp Proc, Vol 353, p 577.

52 GRAMBOW, B, LOIDA, A, DRESSLER, P, GECKEIS, H, DIAZ, P, GAGO, J, CASAS, I and DE PABLO, J
Reaction of high-burnup spent fuel and UO_2 in salt solutions.
Kernforschungszentrum Karlsruhe, 1994 (report KfK 5377).

53 INGEMANSSON, T and ELKERT, J
Model for calculation of absorbed alpha and beta radiation dose to water in contact with highly burnt up nuclear fuel.
ABB Atom, 1991 (report RM 91-23).

54 CHRISTENSEN, H and SUNDER, S
An evaluation of water layer thickness effective in the oxidation of UO_2 fuel due to radiolysis of water.
J Nucl Mater 238 (1996) 70-77, AECL-11479.

55 SUNDER, S
Alpha, beta and gamma dose rates in water in contact with used CANDU UO_2 fuel.
Atomic Energy of Canada Limited Report 1995 (AECL-11380, COG-95-340).

56 JOHNSON, L H, LENEVEU, D M, KING, F, SHOESMITH, D W, KOLAR, M, OSCARSON, D W, SUNDER, S, ONOFREI, C, and CROSTHWAITE, J L
The disposal of Canada's nuclear fuel waste: A study of post-closure safety of in-room emplacement of used CANDU fuel in copper containers in permeable plutonic rock. Volume 2: Vault model.
Atomic Energy of Canada Limited Report 1996 (AECL-111494-2, COG-95-552-2).

57 CHRISTENSEN, H
Calculations Simulating Spent-fuel Leaching Experiments.
To be published in Nucl. Technol., Nov 1998.

Table 1
Comparison of calculated and measured corrosion rates.

Solution[a]	Dose rate	Corrosion rate, µg cm^{-2} d^{-1}	
	Gy h^{-1}	Calculations	Experiments
Ar-purged	5	0.003	n.a*
Ar-purged	120		4.7E-3
Ar-purged	280	0.12	0.10
N_2O-purged	5	0.04	n.a*
N_2O-purged	110		4.4E-2
N_2O-purged	280	0.84	0.36
N_2O-purged	600		3
O_2-purged	0	2.7E-3	3.8E-3
O_2-purged	5	0.06	0.13
O_2-purged	100		0.17
O_2-purged	280	0.84	0.75
O_2-purged	600		3
H_2O_2 10^{-6} M[b]	0	2.2×10^{-4}	2.1×10^{-4}
H_2O_2 2×10^{-4} M[b]	0	0.13	0.13
H_2O_2 3×10^{-4} M[b]	0		0.18
H_2O_2 5×10^{-2} M[b]	0	13	5

[a] Base solution is 0.1 mol dm^{-3} $NaClO_4$, pH 9.5.
[b] Ar-purged, M is mol · dm^{-3}
n.a not applicable: The corrosion potential < -100 mV (SCE)

Table 2
Corrosion rates in α-irradiated, Ar-saturated solutions.

α-source		Corr.pot.	Corrosion rate, $\mu g\ cm^{-2}\ d^{-1}$	
μ Ci	Gy/h	mV SCE	Measured	Calculated
4.7	37	-90	1.1 E-4	3.2 E-2
50	400	10	4.5 E-3	0.33
100	790	40	1.4 E-2	
250	1980	90	8.9 E-2	1.5
686	5440	115	0.21	2.9

Table 3
Reaction mechanism of UO_2 oxidation.

Number	Reaction[a]						Rate constant[b]
1	OH	$+H_2$	$=H$	$+H_2O$			$k_1=3.400\times10^{7}$
2	OH	$+H_2O_2$	$=HO_2$	$+H_2O$			$k_2=2.700\times10^{7}$
3	OH	$+O_2^-$	$=O_2$	$+OH^-$			$k_3=9.000\times10^{9}$
4	H	$+O_2$	$=HO_2$				$k_4=1.800\times10^{10}$
5	H	$+O_2^-$	$=HO_2^-$				$k_5=2.000\times10^{10}$
6	e^-	$+O_2$	$=O_2^-$				$k_6=1.900\times10^{10}$
7	e^-	$+H_2O_2$	$=OH$	$+OH^-$			$k_7=1.200\times10^{10}$
8	c^-	$+O_2^-$	$=HO_2^-$	$+OH^-$	$-H_2O$		$k_8=1.300\times10^{10}$
9	e^-	$+H^+$	$=H$				$k_9=2.200\times10^{10}$
10	e^-	$+H_2O$	$=H$	$+OH^-$			$k_{10}=2.000\times10^{1}$
11	c^-	$+HO_2^-$	$=O^-$	$+OH^-$			$k_{11}=3.500\times10^{9}$
12	OH	$+HO_2$	$=H_2O$	$+O_2$			$k_{12}=7.900\times10^{9}$
13	OH	$+OH$	$=H_2O_2$				$k_{13}=5.500\times10^{9}$
14	H	$+HO_2$	$=H_2O_2$				$k_{14}=2.000\times10^{10}$
15	H	$+H_2O_2$	$=H_2O$	$+OH$			$k_{15}=6.000\times10^{7}$
16	H	$+OH^-$	$=e^-$	$+H_2O$			$k_{16}=1.500\times10^{7}$
17	HO_2	$+O_2^-$	$=O_2$	$+HO_2^-$			$k_{17}=9.600\times10^{7}$
18	HO_2	$+HO_2$	$=H_2O_2$	$+O_2$			$k_{18}=8.400\times10^{5}$
19	H^+	$+O_2^-$	$=HO_2$				$k_{19}=4.500\times10^{10}$
20	HO_2		$=H^+$	$+O_2^-$			$k_{20}=8.000\times10^{5}$
21	H^+	$+HO_2^-$	$=H_2O_2$				$k_{21}=2.000\times10^{10}$
22	H_2O_2		$=H^+$	$+HO_2^-$			$k_{22}=3.560\times10^{-2}$
23	OH	$+OH^-$	$=H_2O$	$+O^-$			$k_{23}=1.200\times10^{10}$
24	O^-	$+H_2O$	$=OH$	$+OH^-$			$k_{24}=9.300\times10^{7}$
25	H^+	$+OH^-$	$=H_2O$				$k_{25}=1.430\times10^{11}$
26	H_2O		$=H^+$	$+OH^-$			$k_{26}=2.574\times10^{-5}$
27	e^-	$+OH$	$=OH^-$				$k_{27}=3.000\times10^{10}$
28	H	$+OH$	$=H_2O$				$k_{28}=2.000\times10^{10}$
29	H	$+H$	$=H_2$				$k_{29}=1.000\times10^{10}$
30	e^-	$+H$	$=H_2$	$+OH^-$	$-H_2O$		$k_{30}=2.500\times10^{10}$
31	OH	$+HO_2^-$	$=HO_2$	$+OH^-$			$k_{31}=5.000\times10^{9}$
32	UO_2	$+OH$	$=UO_3H$				$k_{32}=4.000\times10^{8}$
33	UO_2	$+H_2O_2$	$=UO_3H$	$+OH$			$k_{33}=2.000\times10^{-1}$
34	UO_2	$+HO_2$	$=UO_3H$	$+H_2O_2$	$-H_2O$		$k_{34}=2.000\times10^{8}$
35	UO_2	$+O_2^-$	$=UO_3H$	$+HO_2^-$	$-H_2O$		$k_{35}=2.000\times10^{8}$
36	UO_3H	$+UO_3H$	$=UO_3$	$+UO_2$	$+H_2O$		$k_{36}=1.000\times10^{-1}$
37	UO_3H	$+OH$	$=UO_3$	$+H_2O$			$k_{37}=8.000\times10^{8}$
38	UO_3H	$+e^-$	$=UO_2$	$+OH^-$			$k_{38}=5.000\times10^{8}$
39	UO_3H	$+H_2O_2$	$=UO_3$	$+H_2O$	$+OH$		$k_{39}=2.000\times10^{-1}$
40	UO_3H	$+O_2^-$	$=UO_3$	$+HO_2^-$			$k_{40}=4.000\times10^{8}$
41	UO_3H	$+HO_2$	$=UO_3$	$+H_2O_2$			$k_{41}=4.000\times10^{8}$
42	UO_3	$+e^-$	$=UO_3H$	$+OH^-$	$-H_2O$		$k_{42}=5.000\times10^{8}$
43	UO_3	$+O_2^-$	$=UO_3^-$	$+O_2$			$k_{43}=4.000\times10^{7}$
44	UO_3^-	$+H_2O$	$=UO_3H$	$+OH^-$			$k_{44}=1.000\times10^{1}$
45	UO_3H	$+H$	$=UO_2$	$+H_2O$			$k_{45}=4.500\times10^{6}$
46	UO_3	$+H$	$=UO_3H$				$k_{46}=4.500\times10^{6}$
47	UO_3	$+HO_2$	$=UO_3H$	$+O_2$			$k_{47}=4.000\times10^{7}$
48	O_2		$=O_2D$				$k_{48}=2.100\times10^{-1}$
49	H_2		$=H_2D$				$k_{49}=3.500\times10^{-1}$
50	H_2O_2		$=H_2O$	$+O$			$k_{50}=1.000\times10^{-3}$
51	O	$+O$	$=O_2$				$k_{51}=1.000\times10^{9}$
52	N_2O	$+e^-$	$=N_2$	$+OH$	$+OH^-$	$-H_2O$	$k_{52}=6.000\times10^{9}$
53	HCOOK	$+OH$	$=CO_2^-$	$+H_2O$	$+K^+$		$k_{53}=2.000\times10^{9}$
54	CO_2^-	$+O_2$	$=O_2^-$	$+CO_2$			$k_{54}=6.000\times10^{9}$
55	CO_2	$+H_2O$	$=HCO_3^-$	$+H^+$			$k_{55}=1.000\times10^{3}$
56	UO_3		$=UO_3D$				$k_{56}=4.000\times10^{-4}$
57	UO_2	$+O_2$	$=UO_3H$	$+HO_2$	$-H_2O$		$k_{57}=1.000\times10^{-3}$
58	UO_3H	$+O_2$	$=UO_3$	$+HO_2$			$k_{58}=1.000\times10^{-3}$
59	UO_2		$=UO_2D$				$k_{59}=7.000\times10^{-4}$
60	UO_2D		$=UO_2$				$k_{60}=3.500\times10^{-7}$

[a] UO_3D represents UO_3 diffusing out of the reaction layer near the UO_2 surface (reaction 56), see text (Section 3.4); UO_2D represents a dummy species used to maintain the supply of UO_2 in the reaction layer (reactions 59 and 60), see ref. 16.
[b] Rates are in units of $(\text{mol l})^{-1}\ s^{-1}$ for second-order reactions; reaction rates are for room temperature.

Table 4
G values for gamma and alpha irradiation of neutral water used in the model.

Species	G-value	
	Gamma	Alpha
OH	2.67	0.24
E^-	2.66	0.06
H^+	2.76	0.30
H	0.55	0.21
H_2	0.45	1.30
H_2O_2	0.72	0.985
OH^-	0.1	0.02
H_2O	-6.87	-2.71
O^-_2	0	0.22

Table 5
Comparison of experimental and calculated times for the formation of a $UO_{2.33}$ film on UO_2.

Solution[a]	Dose rate	Time, h	
	Gy h^{-1}	Calculated[b]	Experimental[c]
Ar-purged	5	25	19
Ar-purged	280	2	2
N_2O-purged	5	25	9
N_2O-purged	280	0.2	0.5
O_2-purged	5	20	1.6
O_2-purged	280	0.2	0.15
O_2-purged	0	17	3
H_2O_2 10^{-6} mol dm^{-3}	0	> 40	8
H_2O_2 $2x10^{-4}$ mol dm^{-3}	0	0.8	0.02

[a] Base solution is 0.1 mol dm^{-3} $NaClO_4$, pH 9.5.
[b] Time to reach 90% steady-state concentration of UO_3H species.
[c] Time taken to reach a corrosion potential of -100 mV SCE.

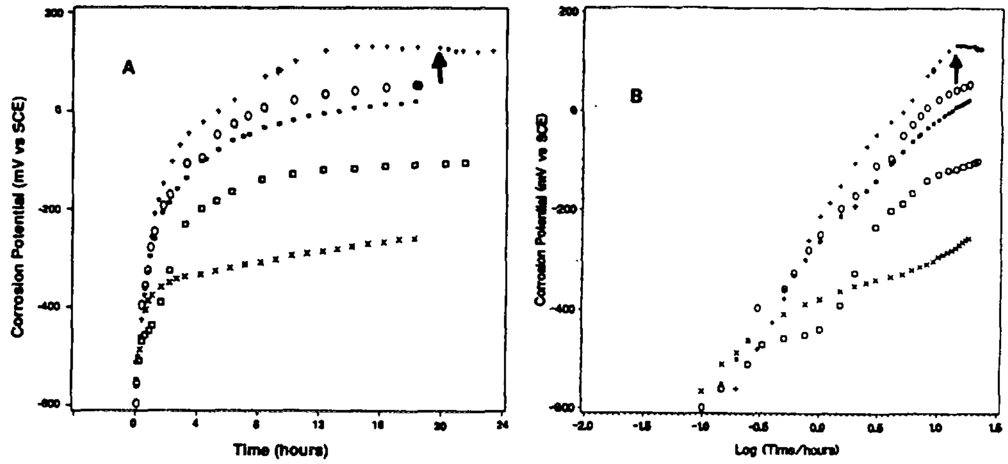

Figure 1
Corrosion potential of a UO_2 electrode in 0.1 mol dm^{-3} $NaClO_4$ solution, pH = 9.5, Ar purge, in gamma fields with absorbed dose rates of 280 Gy/h[+], 29 Gy/h [O], 11 Gy/h [*], 6.4 Gy/h [□], and no field (X), respectively; as a function of (A) time and (B) log time. The arrow indicates the time at which the gamma field was removed. (Reprinted with permission of the copyright holder.)

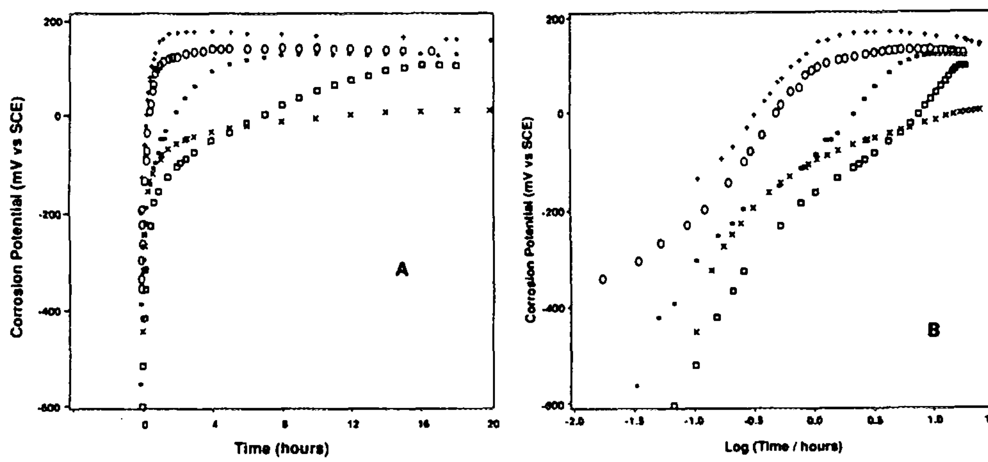

Figure 2
Corrosion potential of a UO_2 electrode as a function of time in O_2-saturated 0.1 $moll^{-1}$ $NaClO_4$ +0.01 $moll^{-1}$ HCOONa solution, pH = 9.5, in gamma fields with absorbed dose rates of 280 Gy/h [+], 23.5 Gy/h [O], 9.5 Gy/h [*], 0.87 Gy/h [□]; and O_2-saturated 0.1 $moll^{-1}$ $NaClO_4$ solution no field (X), respectively; as a function of (A) time and (B) log time. (From Ref 10, reprinted with permission of the copyright holder.)

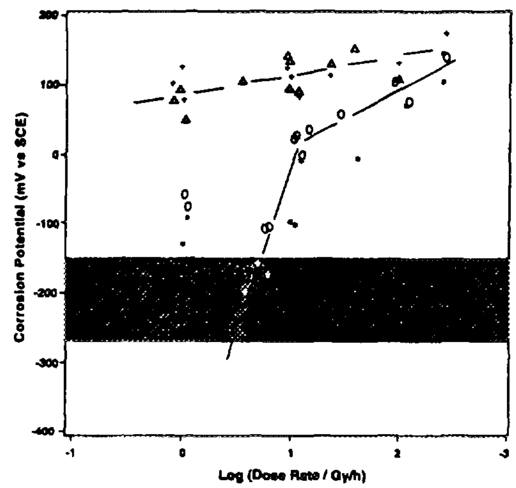

Figure 3
Corrosion potential of a UO_2 electrode as a function of log absorbed dose rate after corrosion for ~18 h in O_2-saturated 0.1 $moll^{-1}$ $NaClO_4$ +0.01 $moll^{-1}$ HCOONa [+], O_2-saturated +0.01 $moll^{-1}$ t-butanol (Δ), N_2O-saturated 0.1 $moll^{-1}$ $NaClO_4$ [*] and Ar-purged 0.1 $moll^{-1}$ $NaClO_4$ solution [O]; all at pH ~ 9.5. The shaded areas show the range of steady-state E_{CORR} values recorded on other UO_2 electrodes in previous experiments in aerated (lighter shaded area) or Ar-purged (darker shaded area) solutions [11, 16-18]. (From Ref 10, reprinted with permission of the copyright holder.)

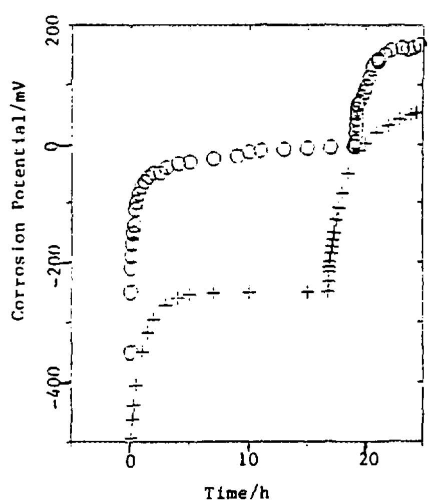

Figure 4
Corrosion potential of a UO_2 electrode in 0.1 $mol \cdot dm^{-3}$ $NaClO_4$ solution, pH = 9.5, (a) air purged, [O]; and (b) Argon purged, [+]; gamma fields were introduced after about 18 h of corrosion without any radiation. (From Ref 3, reprinted with permission of the copyright holder.)

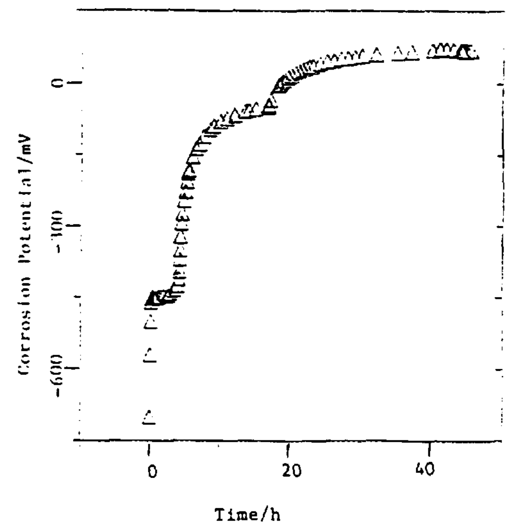

Figure 5
Corrosion potential of a UO_2 electrode in 0.1 mol·dm^{-3} $NaClO_4$ solution, pH = 9.5, containing 1x10^{-6} mol of H_2O_2, argon purge, gamma field of strength 35.1 Gy/h was introduced after 17 h of corrosion without any radiation field. (From Ref 3, reprinted with permission of the copyright holder.)

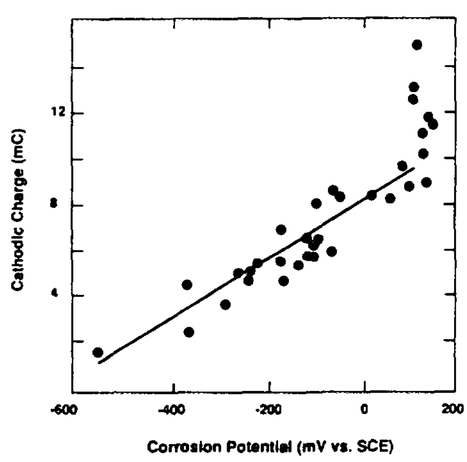

Figure 6
Cathodic charge measured by cathodic-stripping voltammetry (Q_F) at 20 mV/s as a function of the corrosion potential (E_{CORR}) achieved under natural corrosion conditions in 0.1 moll^{-1} $NaClO_4$ (pH = 9.5) solution containing various additives and gamma-irradiated at various absorbed dose rates for various times. (From Ref 10, reprinted with permission of the copyright holder.)

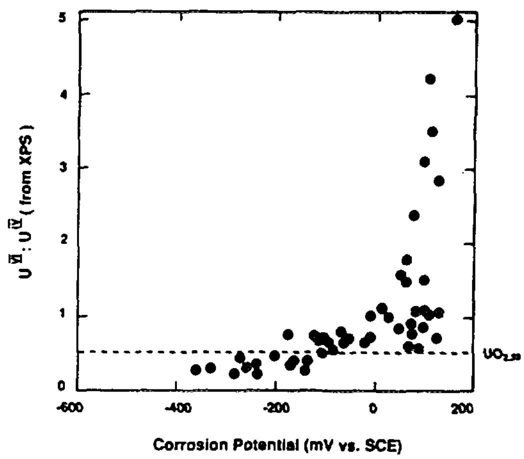

Figur 7
$U^{VI}:U^{IV}$ ratio in the surface of a UO_2 specimen after exposure to gamma-irradiated. (From Ref 10, reprinted with permission of the copyright holder.)

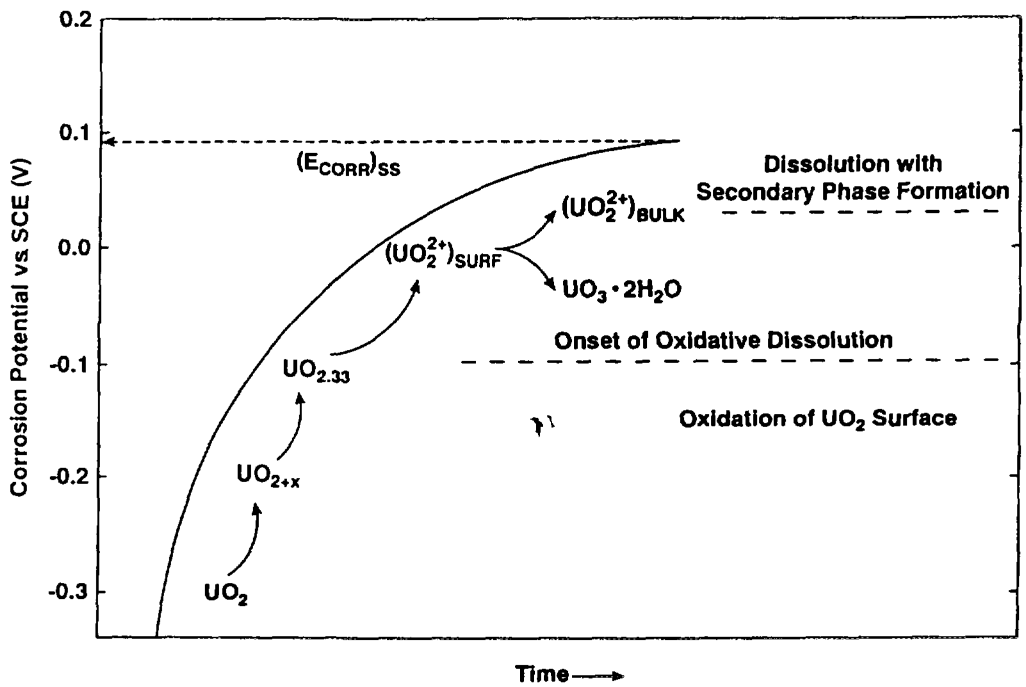

Figure 8
Schematic diagram showing the behavior of the corrosion potential measured on UO_2 electrodes in 0.1 mol l^{-1} $NaClO_4$ solution (approximately pH 9.5). The stages of oxidation and dissolution are also illustrated. (From Ref 12, reprinted with permission of the copyright holder.)

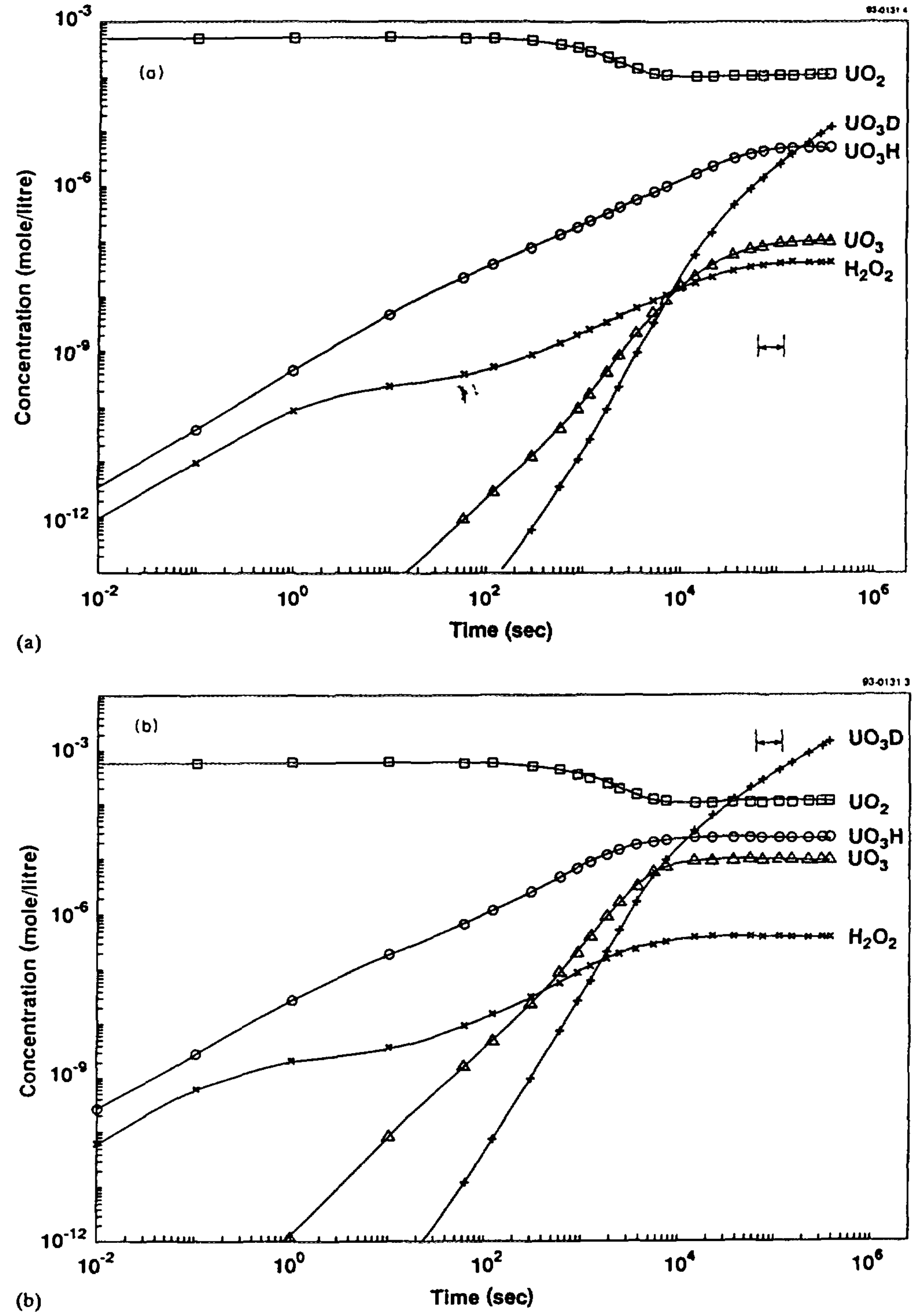

Figure 9
Concentration of selected radiolysis products in solutions with UO_2 and undergoing gamma radiolysis; Ar-purged water, pH 9.5, dose rate (a) 5 Gy h^{-1} and (b) 280 Gy h^{-1}. Arrows define the period over which the dissolution rates were measured (From Ref 12, reprinted with permission of the copyright holder.)

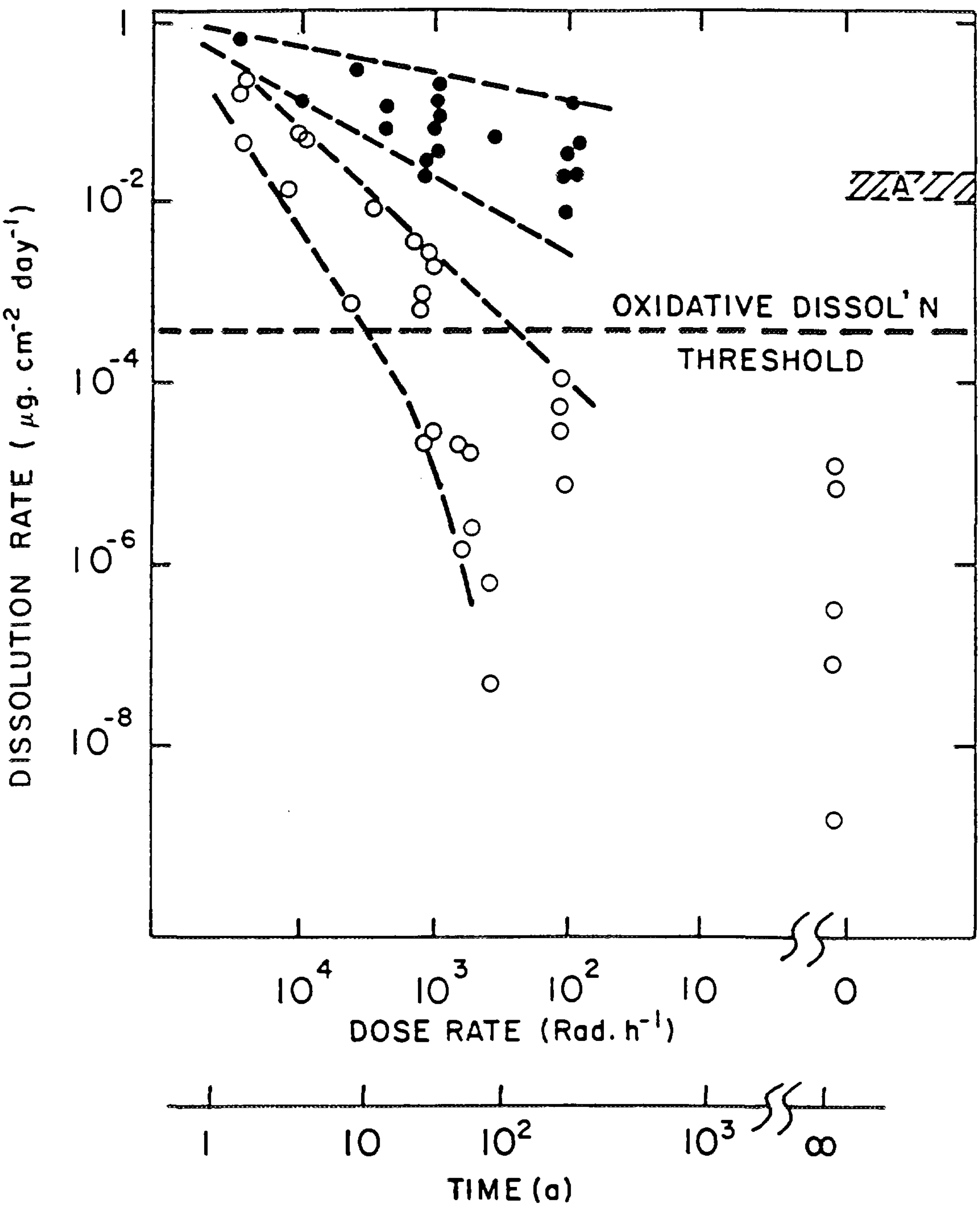

Figure 10
Dissolution rates for UO_2 as a function of the logarithm of gamma dose rate;
O - argon-purged solutions; o - aerated solutions. A is the range of dissolution rates measured in unirradiated but aerated solutions (Shoesmith et al 1989). The time axis represents the times at which such dose rates would be achieved at the surface of a CANDU fuel bundle after being discharged from the reactor (G B Wilkin, unpublished data) (1 rad = 10 mGy). (From Ref 36, reprinted with permission of the copyright holder.)

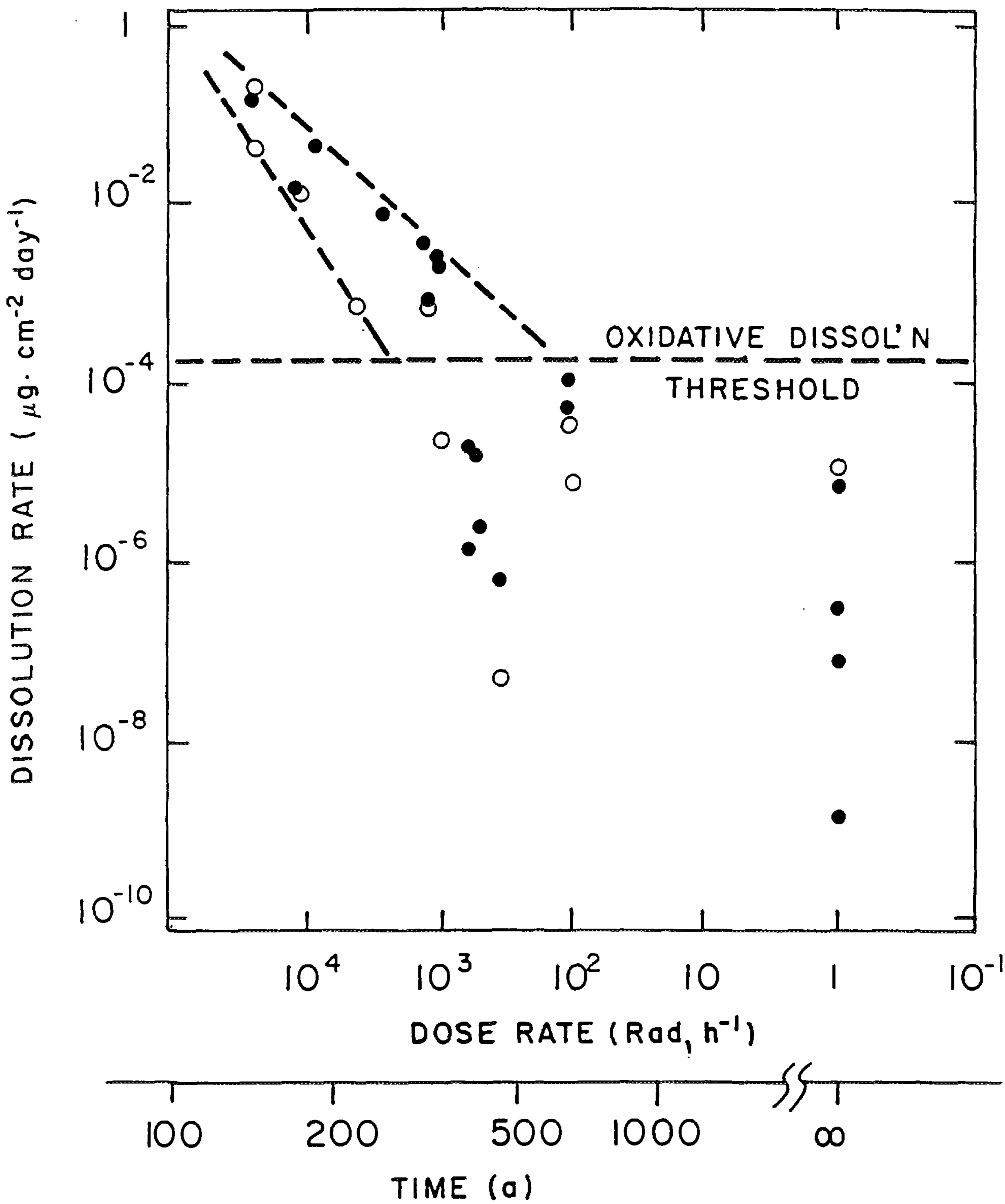

Figure 11
Dissolution rates for UO_2 as a function of the logarithm of beta dose rates for PWR fuel with a burnup of 45 MW·d/kg U on discharge from the reactor (Ingemansson and Elkert 1991). Filled and open symbols indicate two independent sets of data (i rad = 10 mGy). (From Ref 36, reprinted with permission of the copyright holder.)

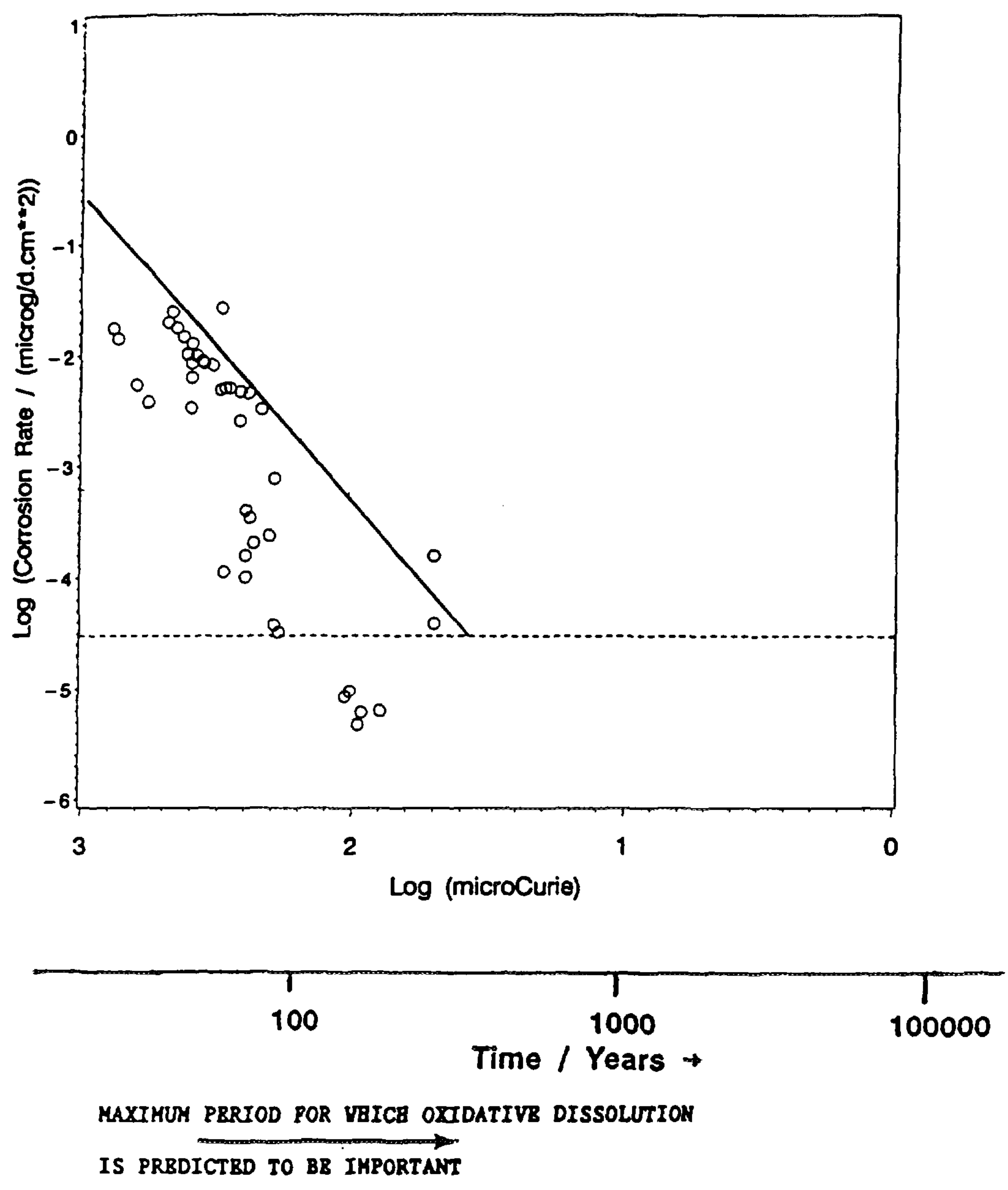

Figure 12
Dissolution rates of UO_2 as a function of alpha source strength in solutions undergoing alpha radiolysis (0.1 mol·dm^{-3} $NaClO_4$, pH = 9.5). The second X-axis (time axis) shows the time at which such activity levels are achieved on the surface of the reference used fuel in the CNFWMP (Bruce CANDU reactor fuel, burnup 685 GJ/kg U). The solid line shows the maximum possible dissolution rate in such a solution; and the horizontal dashed line corresponds to the threshold below which the application of a kinetic model based on electrochemical principles is no longer necessary (see text). (From Ref 37, reprinted with permission of the copyright holder.)

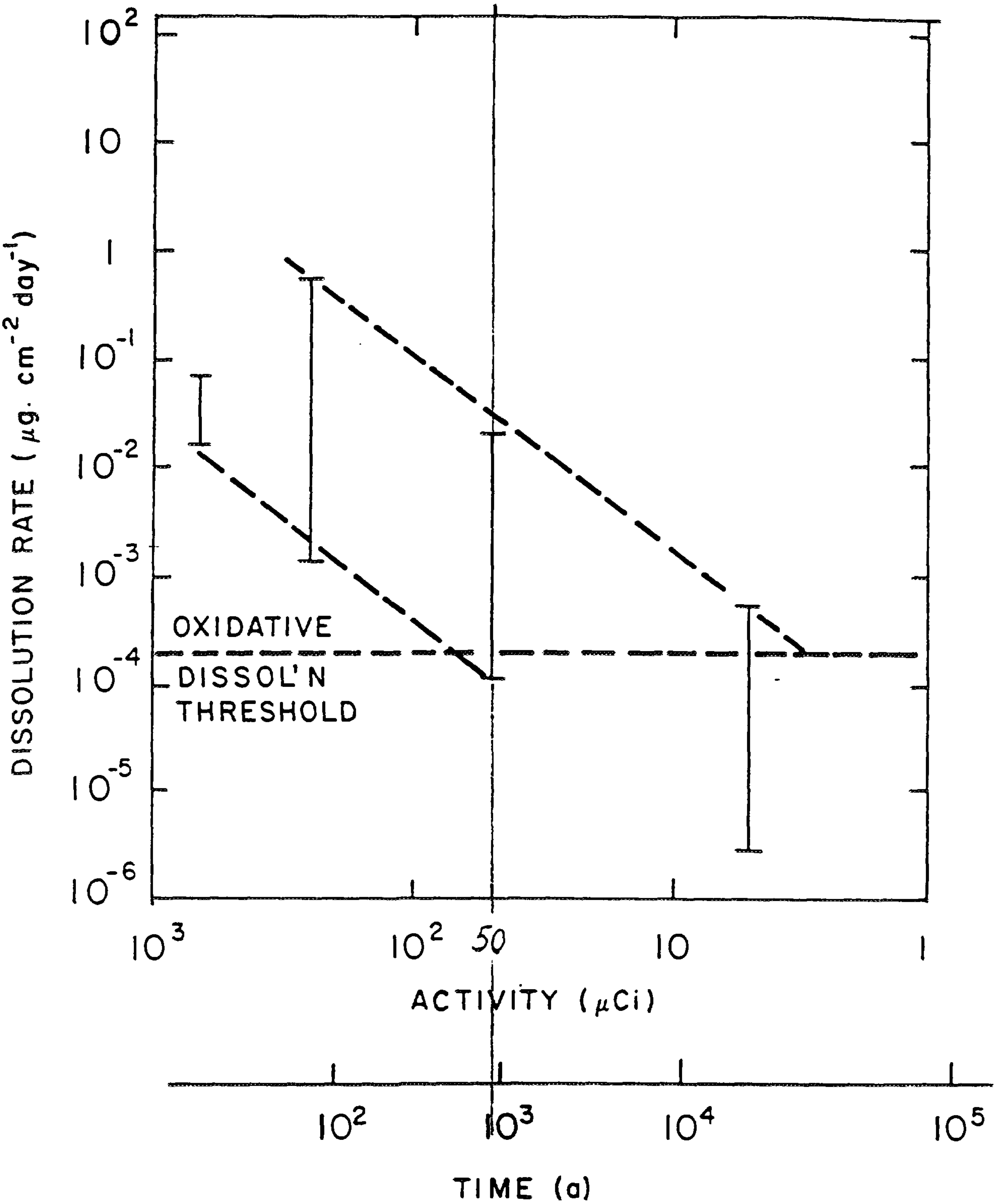

Figure 13
Dissolution rates as a function of the logarithm of alpha source strength. The time axis shows the time at which such activity levels are achieved on the surface of PWR fuel with a burnup of 45 MW·d/kg U on discharge from the reactor (1 Ci = 37 GBq). (From Ref 36, reprinted with permission of the copyright holder.)

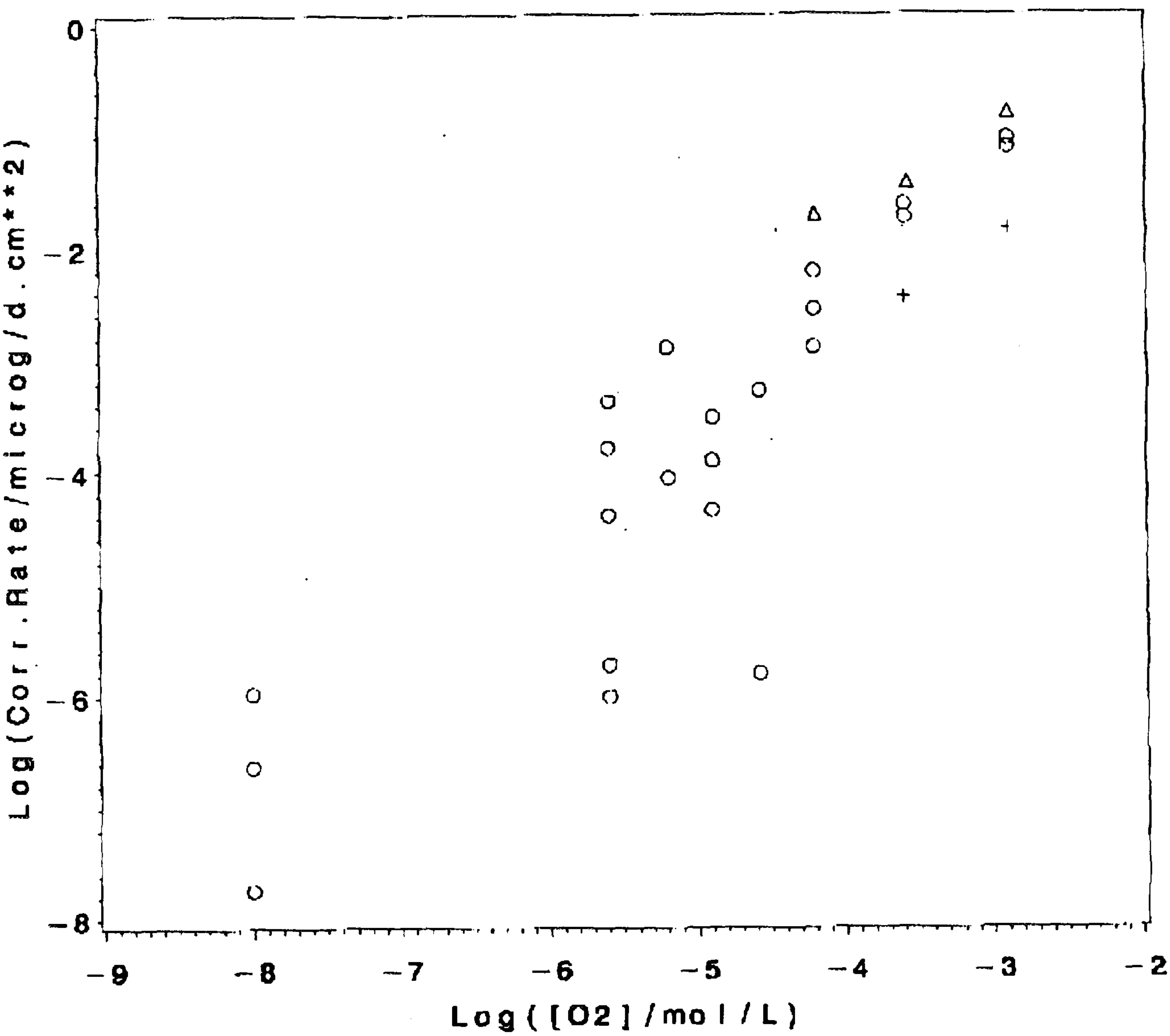

Figure 14
Corrosion rates for UO_2 as a function of dissolved oxygen concentration: O Shoesmith and Sunder [36]; + Grambow et al [41]; and Δ Casa et al [42].

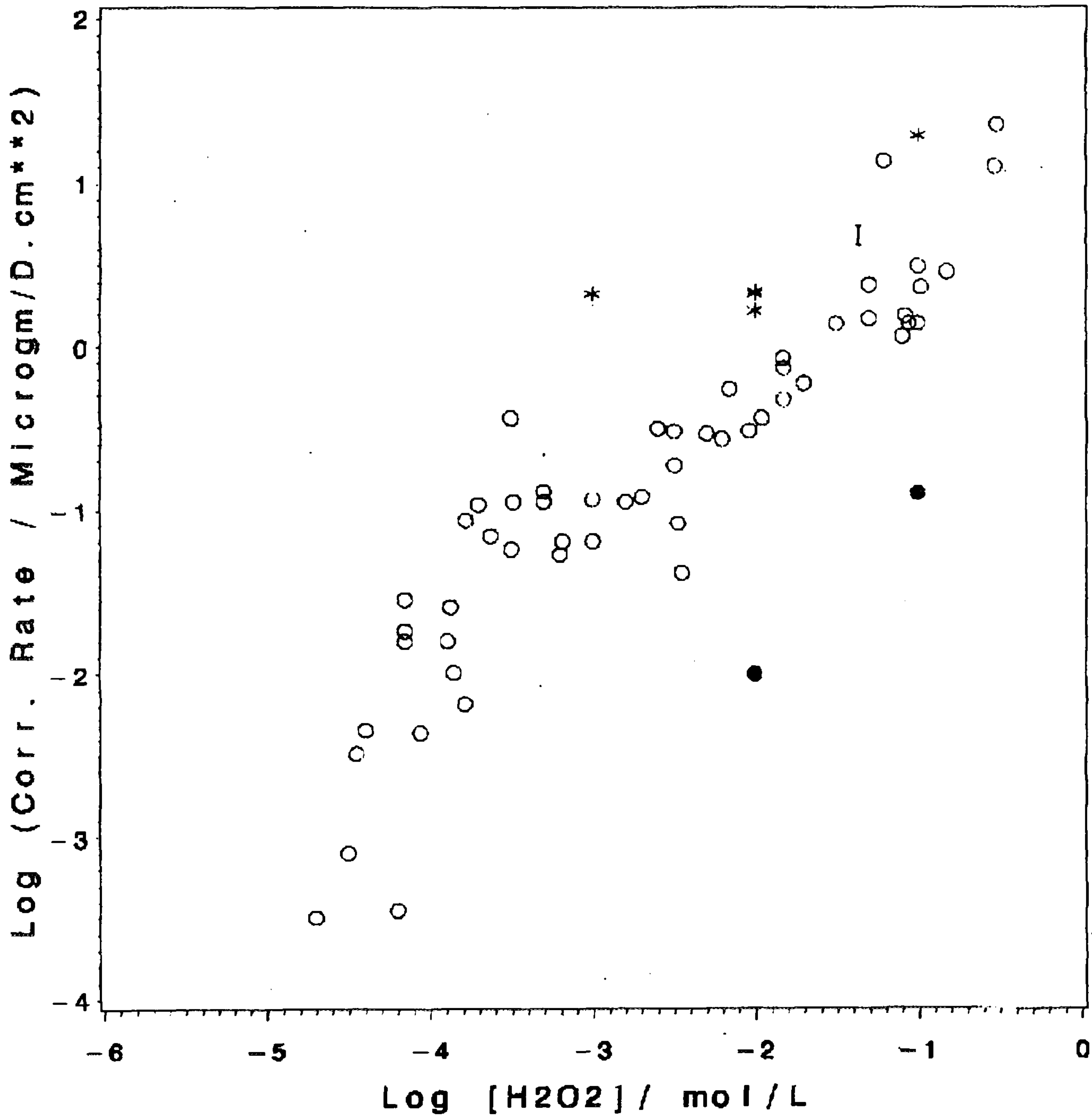

Figure 15
Corrosion rates for UO_2 as a function of hydrogen peroxide concentration: O Shoesmith and Sunder [36]; I Christensen et al [47]; * Gimenez et al [48]; and • Grambow et al [41].

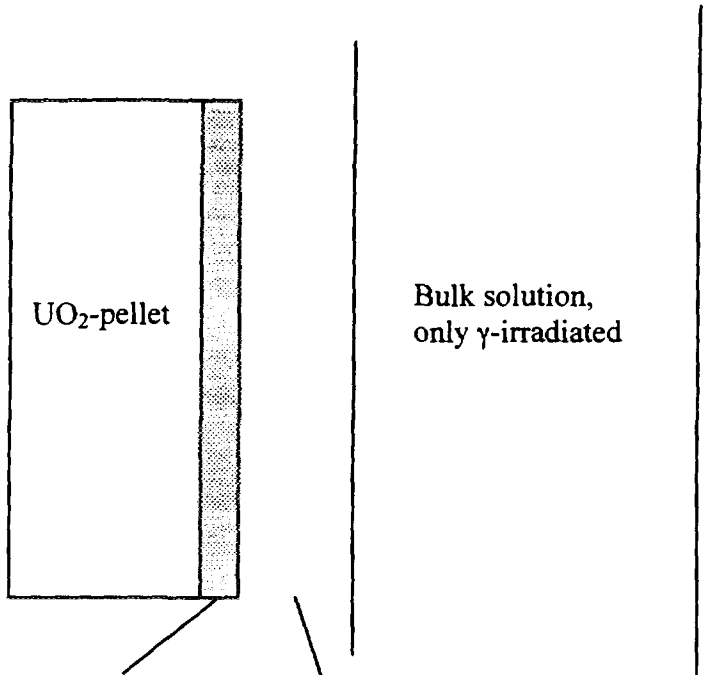

Figure 16
Schematics of the experiments.

STUDSVIK/M-98/71

Current State of Knowledge in Radiolysis Effects on Spent Fuel Corrosion

Hilbert Christensen
Sham Sunder

Studsvik Material

Studsvik Material AB SE-611 82 Nyköping Sweden
Phone +46 155 22 14 00 Telefax +46 155 26 31 50
E-mail material@studsvik.se http://www.studsvik.se